Simultaneous absorption, scattering, and luminescence mappings for the characterization of optical coatings and surfaces

Laurent Gallais and Mireille Commandré

An experimental setup, based on the laser-induced deflection technique, is developed to measure simultaneously the 244 nm laser absorption, scattering, and luminescence on optical components. The different techniques and methods that have been specifically developed to obtain both high resolution (micronic) and sensitivity (a few 10^{-7} of the incident power for the absorption, 10^{-8} for scattering and fluorescence) are presented. Different applications are then explored: the study of losses in deep UV multilayer coatings (HfO_2/SiO_2 mirrors) and the analysis of contamination defects on bare substrate and structural defects in optical coatings.

OCIS codes: 310.0310, 350.5340.

1. Introduction

The quality, in terms of losses and defects, of optical coatings and surfaces is a major point for the development of many optical systems. For instance, the improvement of the laser-induced damage threshold and durability of optical components is required for various applications in the UV[1–4] (fusion ignition, photolithography systems for the semiconductor industry). The problems encountered are often problems of defects on surfaces and coatings that have to be localized, characterized, and identified for the interaction with the laser to be understood and for the manufacturing process to be improved. To obtain results in this field, high-performance characterization tools have been developed,[5–8] but the progress in the process techniques and in the new applications leads to the development of new tools, such as the one we present in this paper, which is based on the localized measurement of the optical losses.

Photothermal tools are largely used for the measurement of low-absorption losses[5,6,9–11] that can be at the origin of the degradation of optics. However, additional measurements such as the scattering[12–15] and the luminescence[16,17] of the optics can give information on the nature of defects. In this way, we chose to develop an apparatus that can combine these three measurements to characterize with both high spatial resolution and detectivity optical components such as superpolished substrates and low-losses coatings.

In Section 2 we present the experimental setup and detail the calibration procedure. In Section 3 we explore the experimental and theoretical capabilities of the apparatus in terms of resolution, detectivity, and ability to detect isolated defects. We discuss, in Section 4, different applications that illustrate the potentialities of the apparatus.

2. Materials and Methods

A. Experimental Setup

The experimental setup is detailed in Fig. 1. It involves a 488 nm argon laser doubled at 244 nm with an external cavity frequency doubler. The beam is modulated (10 Hz–20 kHz) spatially filtered, and focused on the sample through different lenses, depending on the required pump-beam diameter (from 3 to 100 μm). The position and size of the image waists of the pump and probe beams are checked with the knife-edge technique (measurements are given in Fig. 2).

Absorption measurements are performed with the photothermal deflection (PD) technique implemented in transmission (also called collinear configuration).[18,19] The absorption of the modulated pump

The authors are with the Institut Fresnel, Unité Mixte de Recherche, Ecole Généraliste d'Ingénieurs de Marseille - Aix Marseille I - Aix Marseille III, Domaine Universitaire de Saint Jerome, 13397, Marseille Cedex 20, France. L. Gallais' e-mail address is laurent.gallais@fresnel.fr.

Received 1 March 2005; accepted 29 June 2005.
0003-6935/06/071416-09$15.00/0

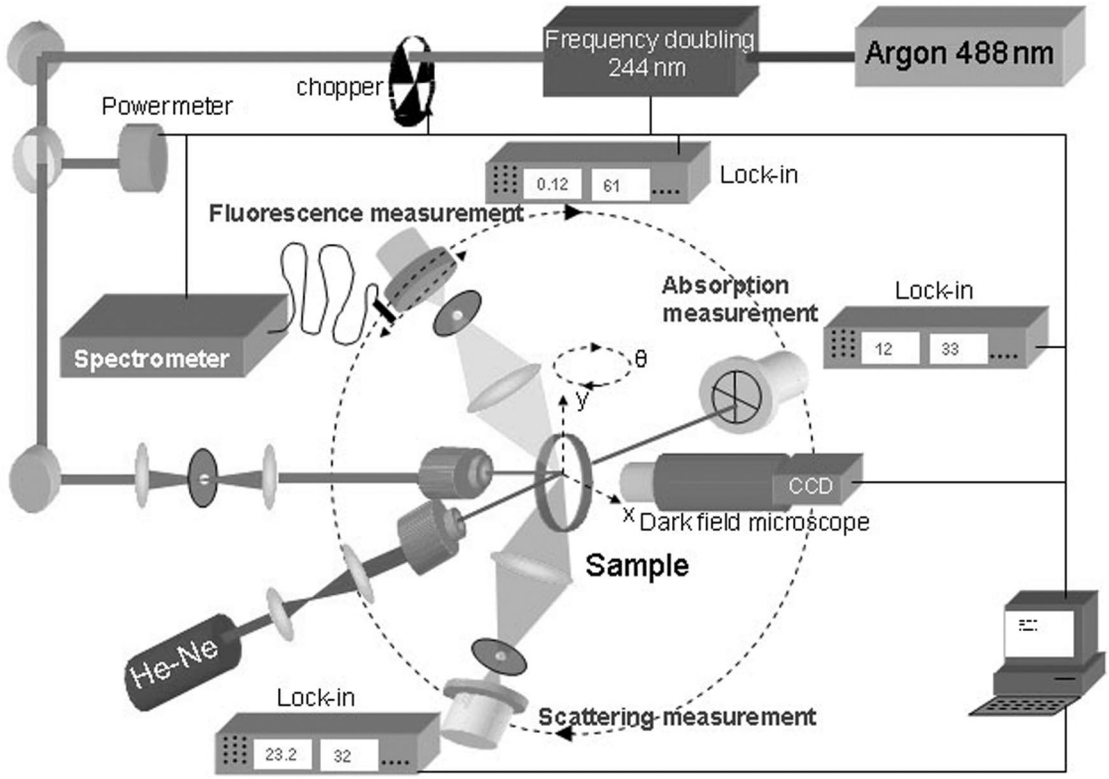

Fig. 1. Experimental setup.

beam induces a periodic local heating that causes refractive index gradients to appear in the air and in the material. A second laser beam, called the probe beam (He–Ne in our case), passes through the heated area and is then deflected by the modulated refractive index gradient and/or by the bumped surface. The resulting deflection, measured by a position sensor, directly depends on the optical absorption. The calibration procedure needed to obtain the absorption value from the measured deflection of the probe beam is described in Subsection 2.B.

For scattering measurement, a lens collects part of the pump light scattered in a 20° cone out of the specular direction, which is measured with a photodetector. A pinhole is placed in the focal plane of the lens to avoid light scattering from the rear face of the sample. The same configuration is used for luminescence measurement to measure light emitted in the visible range, with adapted filters to eliminate pump and probe beam scattering. Passband filters can be used to map the luminescence at a particular wavelength. The photodetector can be replaced by a spectrometer to analyze the luminescence spectrum of an area of interest.

Absorption, scattering, and luminescence mappings are performed simultaneously in exactly the same experimental conditions and are corrected of temporal fluctuations of the pump power. The minimum sampling step of the mappings is 1 μm.

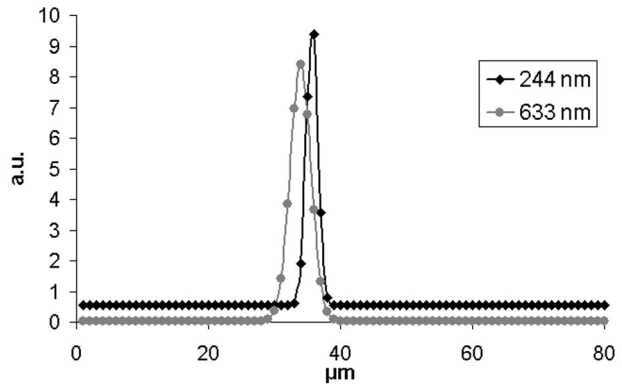

Fig. 2. Measurement of the pump- and probe-beam profiles in the plane of the sample. Case of a 3 μm pump beam and a 6 μm probe beam.

B. Calibration of the Absorption Measurement

In the case of the absorption measurement, the measurement is indirect (measurement of the probe beam deflection) and depends on the optical and thermal parameters of the sample (often not known), so that the calibration is not a trivial problem. It is the main limitation of the accuracy of absolute absorption measurement with the PD technique.[5,9] Consequently, we detail in the following part the procedure that we have adopted.

1. Method

The deflection of the probe beam is directly related to the absorbed optical power in the sample, and the photothermal signal (PS) of a sample is related to its absorptance by the relation $A = C$ PS, where C is a

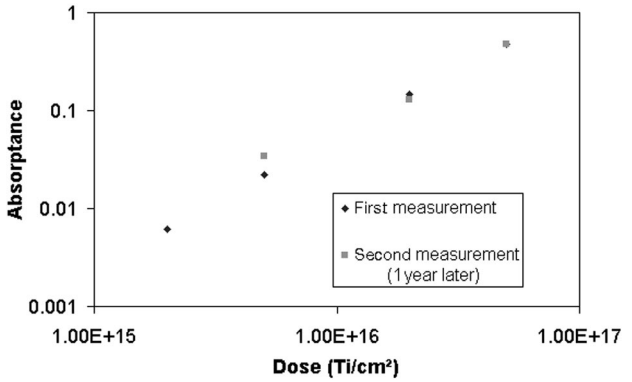

Fig. 3. Absorption measurements by spectrophotometry of ion-implanted samples.

Table 1. Range of Values for the Thin-Film Parameters[a]

Parameters	Minimum	Maximum	Typical
Real Index (n)	1.3	3	2.3
Imaginary Index (k)	10^{-10}	10^{-1}	10^{-4}
Thickness (e)	10 nm	10 μm	100 nm
Thermo-optic coefficient (dn/dT) K^{-1}	-10^{-4}	10^{-4}	$2 * 10^{-5}$
Conductivity (K) $W\ m^{-1}\ K^{-1}$	0.01	10	0.1
Calorific capacity (ρC) $J\ m^{-3}\ K^{-1}$	5×10^5	5×10^6	10^6
Layer–Substrate Interface Resistance (R) $m^2\ K\ W^{-1}$	0	10^{-5}	0

[a] Typical values used in the calculation.

constant, depending on the sample properties and experimental conditions.

In the case of thin films or surfaces, a classical solution for the calibration is the use of a sample of known absorption.[18,19] The calibration procedure is then based on the comparison of the signal of the sample (S) under study with a calibration sample (CS) of well-known absorptance. We have

$$A_{CS} = C_{CS}\,PS_{CS}, \tag{1}$$

$$A_S = C_S\,PS_S. \tag{2}$$

Therefore the problem of calibration is to find experimental conditions and a calibration sample adapted to the tested sample so that the ratio $K = C_S/C_{CS}$ depends only on well-known experimental conditions and optical and thermal parameters and is independent of unknown parameters. Then this calibration constant K can be calculated, and the absorptance of the sample can be deduced as follows:

$$A_S = K\,\frac{PS_S}{PS_{CS}}\,A_{CS}. \tag{3}$$

2. Development of Calibrated Samples

For the calibration sample, an absorbing, deposited thin film can be used with the condition that the substrate has properties similar to the sample to be measured.[18,19] This layer has to be absorbing enough to be measured with a spectrophotometer. However, to have the smallest contribution of the deflection inside the layer, and consequently minimize the dependence of the calibration constant on the layer parameters, this layer has to be as thin as possible.

One solution for obtaining absorbing layers consists of depositing an oxide layer with a classical evaporation process and adjusting the partial oxygen pressure to obtain nonstochiometric layers.[18,19] However, the absorption value, as well as the repeatability, is difficult to control. In addition layer properties can change with time or laser irradiation. To avoid such problems we chose to obtain our absorbing layer by ion implantation on nonabsorbing materials. Indeed the main advantages of this technology are the repeatability and the homogeneity achieved as well as the ability to control the absorption level by adjusting the implantation dose.[20]

We made different absorbing samples by Titanium implantation on fused-silica substrates. The implantations were performed with the following conditions: ion dose = 5×10^{16}; 2×10^{16}; 5×10^{15}; 2×10^{15} cm^{-2}, implantation energy = 70 keV. Under these conditions, the thickness of the implanted Titanium layer is approximately 100 nm.[20] The samples have been measured by spectrophotometry and to investigate the long-term stability of such samples, we repeat these measurements after 1 yr. The absorptance values are reported in Fig. 3 (measurement is a mean value on few square millimeters of the sample surface). We observe no significant aging effect on the samples.

3. Measurement Accuracy

As we have seen previously, the absolute measurement of absorption requires the calculation of the calibration constant. However, for materials in thin-film forms, we lack accurate numerical values for their optical and thermal properties. We can calculate the influence of these different parameters on the calibration to evaluate the uncertainty on our absorption measurement and to find experimental conditions for which their possible variations have little influence.

The theoretical approach of PD has been described in detail in different papers.[9,18,21,22] For our application, we used the modeling described by Commandré *et al.* in Ref. 9 and relied on the following hypothesis: the sample is infinite in both the x and the y directions; the pump beam is Gaussian and normal to the sample surface; conduction exists only in heat transfers; temperature distribution is unaffected by the thermal buckling of the sample; and the acoustic wave that accompanies the rise in temperature has no effect. Under these conditions, the heat source due to the optical absorption in the material is obtained; then the effects of tempera-

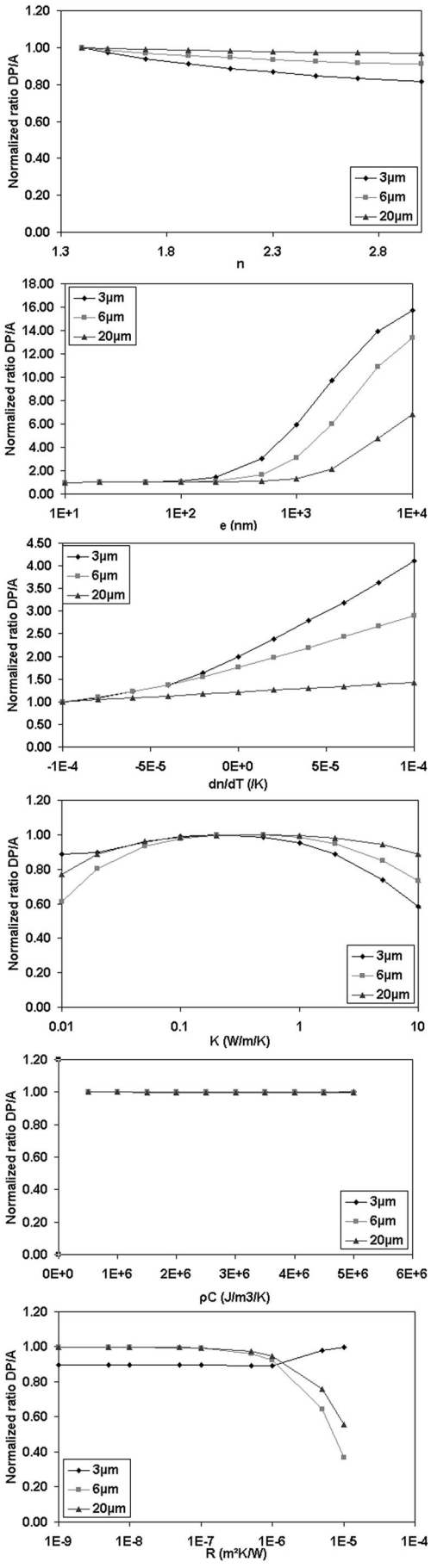

ture distribution on the probe-beam distribution can be calculated for each medium i (air, layer, substrate)

$$PD_i = \frac{1}{n_i}\frac{\partial n_i}{\partial T}\int_{\text{path } i}\left[\frac{\partial T_i}{\partial x}(x,\ y,\ z,\ t)\right]_{x=x_0,\ y=y_0} \mathrm{d}z, \quad (4)$$

where (x_0, y_0) is the shift between the centers of the pump and probe beams in the plane $z = 0$. In the transmission configuration, the total PD is the sum of complex deflections in the three media.

We calculated the influence of thin-film properties (refractive index, conductivity, thermo-optic coefficient, calorific capacity, interfacial resistance) on the ratio of the PD to the layer absorption for a typical thin film whose properties are given in Table 1 (last column). The range of values for these parameters found in publications[23–30] are reported in Table 1 (columns 1 and 2). The results for our experimental conditions and for different pump-beam sizes are plotted in Fig. 4.

On the different plots, we observe that the more focused the beam and thicker layer, the more sensitive we are to variations in the layer optical; or thermal parameters, which complicates the calibration procedure in these cases. For instance, for a 20 µm beam it can be difficult to compare films with thicknesses greater than 1 µm, but for films thinner than 1 µm, it is possible to perform a measurement of the absolute absorption with less that 20% error without any knowledge on the film properties. Of course, this is an extreme value, and the better the knowledge of the layer, the more accurate the measurement. However, in the case of a highly focused beam the calibration can be more complicated; in this case we must either use a calibration sample with the same properties of the sample to be measured or calculate the ratio between the two signals (K value of Subsection 2.B), which implies a good knowledge of the index and the thickness of the layer, which is quite easy, and the thermo-optic coefficient and conductivity, which is more complicated but can be done with several techniques.[24–30]

Then it is possible and valid to perform a calibration of the PD, with 10% to 20% for a reasonable value of the accuracy. A limitation occurs for the measurement of multilayer components; indeed in this case the thickness is often greater than 1 µm, and interference effects have to be taken into account. For this application, knowing the absolute absorption requires the extension of our photothermal model to calculate the calibration constant, which has been done.[31]

Fig. 4. Variation of the PD signal with the thin-film parameters. Calculations made for the case of an absorbing thin film on a nonabsorbing substrate (F = 1500 Hz), for different probe-beam sizes.

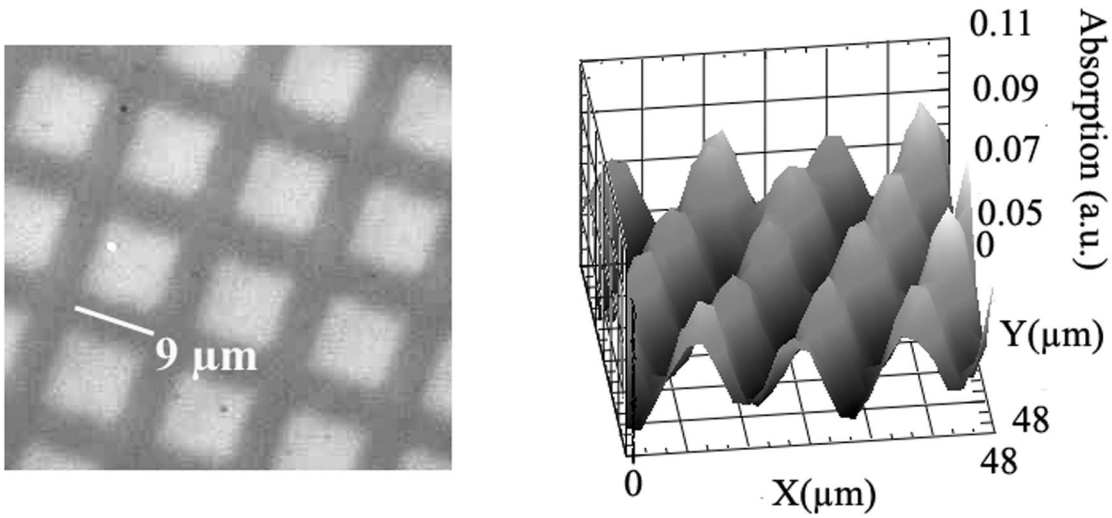

Fig. 5. (a) Nomarski image of the implanted sample. (b) Absorption mapping of the same sample (pump = 3 μm, probe = 6 μm).

C. Calibration of the Scattering and Luminescence Measurement

As we have seen in the experimental setup description (Section 2), the scattering measurement is a partial measurement of the total scattering in an arbitrary angle. In the mappings, we represent a partial scattering coefficient, defined as the ratio of scattered light power in the 20° cone to the measured power of the incident pump beam. This ratio between two powers is difficult to relate to the total scattering, which is usually measured and for which several standardized measurement procedures exist,[32] given that there is no direct correlation between the partial and the direct scattering for an ordinary sample. However, measurements can be easily converted in terms of a total integrated scattering (TIS) value that would corresponds to a Lambertian sample.

As concerns the luminescence measurement, the calibration is a difficult problem since the spectral response varies with the sample. In our studies, we are interested only in localizing defects and/or analyzing the spectral signal. Consequently, the mappings are given in arbitrary units.

3. Results

To perform measurement in very high quality components we have to achieve a high sensitivity and a good spatial resolution to be able to localize defects. In this section we present the results in terms of resolution and detectivity for the absorption, scattering, and luminescence measurements. Then we discuss the theoretical limits of the setup for the detection of isolated defects.

A. Resolution

The resolution of the system is related to the size of the pump beam and the sampling step: one way to magnify the resolution is to focus the pump beam on the surface sample and to have the smallest sampling step. This process is all the more interesting as the calculation shows that PD collinear signal increases while the pump beam is focused.[11] In our case the minimal pump-beam size that can be obtained given the compaction of our system is 3 μm, and the minimum sampling step is 1 μm, which means that the resolution (the minimal distance to resolve two absorption maximum) cannot be better than micronic. However, as we will see in Subsection 2.C, the foregoing does not means that isolated submicronic defects cannot be detected.

To check this resolution, we prepared special resolution targets. One target is realized by titanium implantation in a silica substrate through an electronic microscope used as a mask. We obtain an array of absorbing defects. A Nomarski image of this sample is presented in Fig. 5 with the associated photothermal mapping. This photothermal imaging proves that a few micronmeters resolution can be obtained. To explore the limits of the spatial resolution, we made samples with smaller patterns using photoresist deposition on a silica substrate (*demander une ref a ludo*). We obtained with this technique an absorbing grating with a step of 2 μm and a thickness of the lines of 1 μm. A Nomarski image of this sample is presented in Fig. 6, associated with the photothermal image, where the pattern is clearly resolved. Then a micronic resolution can be reached with this apparatus.

B. Detectivity

1. *Absorption*

To reach a good sensitivity, the size of the probe beam has to be small compared with the size of the heated area created in the thin film. Experimentally, the size of our probe beam is fixed to 6 μm. The lowest absorption that we can detect is related to the background noise in the case of a nonabsorbing sample. The noise is studied in the following manner: we performed a mapping with a cutoff pump beam and with the sample placed in the sample holder, which results in a noise mapping for this sample and mea-

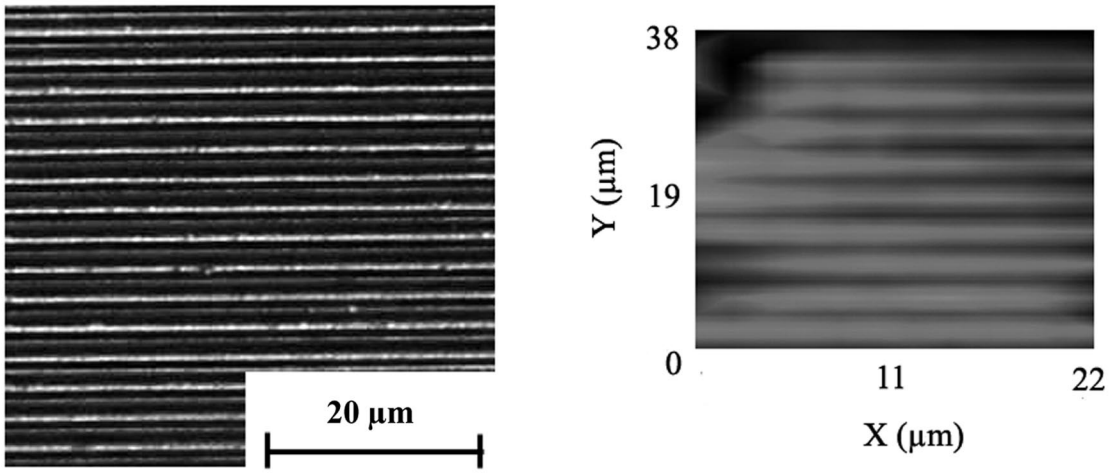

Fig. 6. (a) Nomarski image of the absorbing grating. (b) Absorption mapping of the same sample (pump = 3 μm, probe = 6 μm).

surement conditions. This method takes into account all the noise sources that can occur during the mapping: detection system noise, probe-beam pointing instability, and noise associated with the moving of the sample. The noise-equivalent absorptance equals to 0.4 ppm with 200 mW pump power. One way to improve this value could be to decrease the beam pointing instability of the probe laser or to use another modulation system.[10]

2. Scattering

To estimate the detectivity, we used calibrated scattering samples and compared their measurements to the background noise. The calibrated samples are commercial Lambertian with a TIS of 99%. From our measurements it comes out that the noise-equivalent partial scattering that can be detected corresponds to 6×10^{-8} of the incident power, which compared with an equivalent Lambertian sample would correspond to a 8.5×10^{-4} TIS.

3. Luminescence

In the case of a luminescence signal, it is more difficult to obtain the detectivity since the sensitivity of the detector depends on the wavelength of the luminescence. Typically, however, we can measure a few 10^{-8} of the incident power on this channel at 600 nm.

C. Detection of Isolated Absorbing Defects

We have seen that given the beam size and the sampling step of the setup, the resolution cannot be better than 1 μm; however, we can expect to detect isolated submicronic defects. We propose in this part to estimate the size of the lowest absorbing defect detectable with our apparatus, given the detectivity estimated previously, 0.4 ppm at 244 nm.

If we consider a spherical absorbing particle embedded in an homogeneous nonabsorbing medium, the absorption of the particle can be related to its size and to its complex index, given an appropriate electromagnetic calculation based on Mie Theory[33]:

$$\Delta A = 4\pi\left(\frac{n'n''}{n_s}\right)\beta\left(\frac{\Delta\nu}{\lambda}\right)\left(\frac{d\Phi}{dS}\right). \quad (5)$$

This last relation permits calculation of the power absorbed (ΔA) by a particle of volume $\Delta\nu$ and complex index $n = n' + jn''$, under an irradiation $d\Phi/dS$ at wavelength λ in a surrounding medium with an index n_s. β is a parameter that accounts for interference and resonance effects in the particle.

We plot in Fig. 7 the relation between the size and the imaginary index of a particle embedded in silica that induces a 0.4 ppm absorption at 244 nm, with 200 mW pump power and a 3 μm diameter spot size (with a fixed real index: 2). This give us an estimation of the smallest detectable particle in our measurement conditions.

From these results it can be seen that for highly absorbing particles ($n'' > 1$) a 10 nm particle could be detected; and if the particle is not very absorbing ($<10^{-3}$), particles of a few tens of micrometers to 100 μm could be detected. Of course, these are theo-

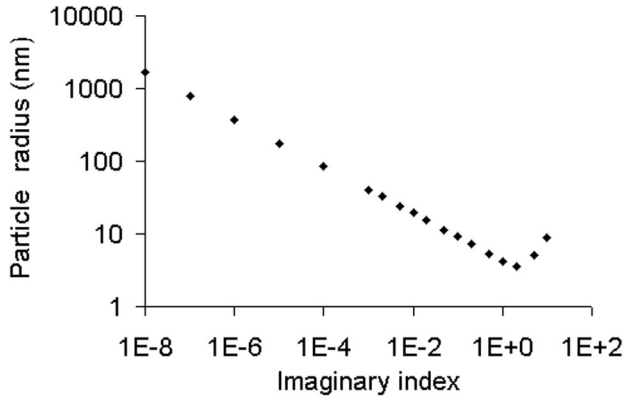

Fig. 7. Particle size as a function of its imaginary index calculated from Eq. (5) in the following conditions: $\Delta A = 4 \times 10^{-7}$, $n' = 2$, $d\phi/dS = 2.8 \times 10^{10}$, $\lambda = 244$ nm, $n_s = 1.52$.

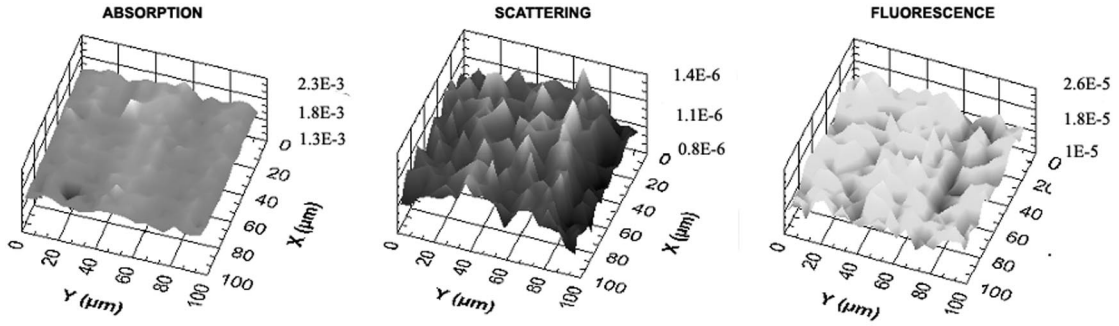

Fig. 8. Absorption, scattering, and fluorescence mappings on HfO_2/SiO_2 mirrors centered at 250 nm.

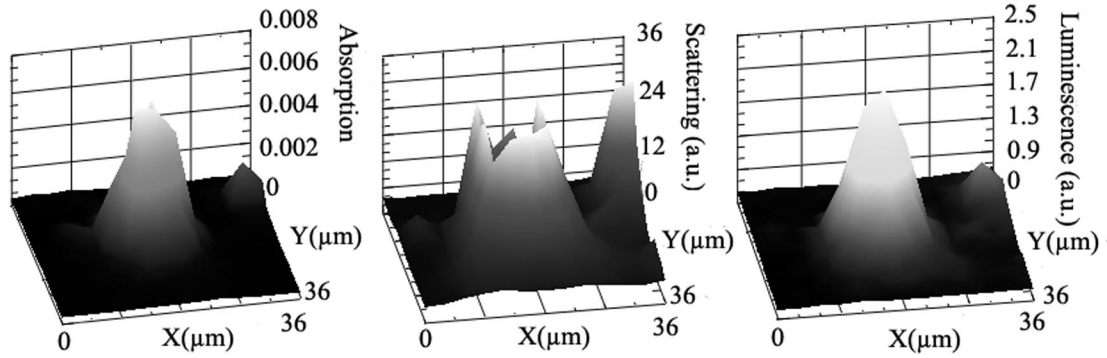

Fig. 9. Absorption, scattering, and fluorescence mappings of a micronic defect on a silica substrate. (The measurement was made with a pump beam of 6 μm diameter; then the result on the mapping is the convolution of the beam profile with the defect.)

retical results, but they give some orders of magnitude of what we should expect with this setup.

4. Applications to Thin Films

A. Characterization of Losses in Deep Ultraviolet Optical Components

A direct application of the setup presented above is the measurement of losses (absorption, scattering, and fluorescence) in deep UV (DUV) optical coatings. We studied HfO2/SiO2 mirrors (centered at 250 nm) made by ion plating at the Institut Fresnel.[34] Mappings of these three measurements are given in Fig. 8. As concerns the absorption, after calibration with a specific procedure adapted to multilayer coatings (see Ref. 32 for more details), a mean value of 5×10^{-3} is found. We observe also a low level of scattering and luminescence losses but these kinds of value are difficult to compare with the literature since to our knowledge it is the first apparatus that can give such data on these materials.

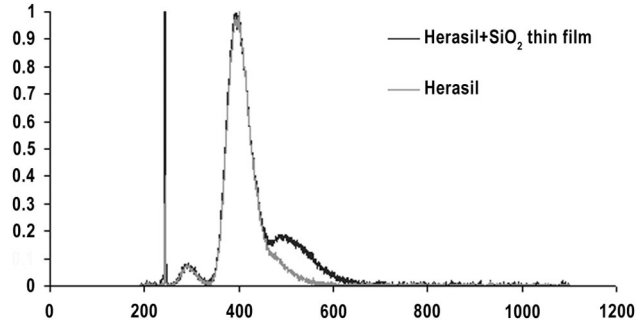

Fig. 10. Luminescence spectra of a Herasil surface and a Herasil surface coated with a SiO_2 thin film, under 244 nm irradiation.

B. Study of Localized Defects on Coatings and Substrates

The main advantages of this apparatus is that high resolution can be obtained and that isolated defects can possibly be detected. These defects can then be characterized in terms of absorption, scattering, and luminescence, giving information on the nature and origin of defects (for instance, by analyzing the luminescence spectrum). An example of such measurement is given in Fig. 9, where we observed a micronic contamination defect on a silica substrate.

C. Luminescence of Optical Thin Films

In addition to the advantages discussed above, it is also possible to analyze the luminescence spectrum with the *in situ* spectrometer. By using a highly focused beam and by imaging the excited area on an optical fiber, it is possible to analyze the area of interest of few micronmeters. Then the luminescence of a micronic defect can be isolated from the surface, or the luminescence of a thin film can be isolated from the substrate. We present this last application in Fig. 10. We record the luminescence signal of a glass surface (Herasil) and the luminescence signal of the same surface coated with a SiO_2 layer (with a me-

chanical thickness of 200 nm, deposited by ion plating). Notice that the thin line on the spectra is due to the scattering of the 244 nm pump laser. On the Herasil substrate, we can clearly see two luminescence bands: the first one at 290–300 nm and the second at 400 nm. These luminescence bands are connected with impurities and intrinsic defects of glasses that have been studied.[35–37] In the case of the SiO_2 layer, apart from the 300 and the 400 nm peaks, a third peak around 490 nm appears. This last luminescence band could be attributed to impurities due to the complicated fabrication process: the thin film is obtained by evaporation of a silicon target under a partial pressure of oxygen and nitrogen (nonbridging oxygen atoms for instance). Because this presence of defects is of critical importance for the performances and characteristics of optical coatings, the luminescence diagnostic could be a useful tool for the control of a coating quality.

5. Conclusion

An apparatus was developed for the simultaneous measurement of absorption, scattering, and luminescence of optical coatings and surfaces at 244 nm. We demonstrated that by the use of an adapted calibration procedure and the development of specific resolution target, calibrated absorptance measurement could be done up to 0.4 ppm, in correlation with scattering and luminescence and with a micronic resolution.

We have shown by different examples that this tool has a great interest for the characterization of losses in DUV optical components and the analysis of contamination or structural defects that can affect the performance and characteristics of optical coatings. We will now focus our attention on the interpretation of these defect luminescence spectra for application in cleaning, fabrication process, and laser damage studies.

We thank Michel Cathelinaud, Ludovic Escoubas, and Philippe Torchio from the Institut Fresnel for their contribution by providing the different samples used in this study. Funding of this work by the Centre Régional de Microélectronique et des Systèmes Intéractifs; the Région Provence-Alpes-Côte d'Azur (PACA), and the Conseil Général des Bouches du Rhone is gratefully acknowledged.

References

1. G. Ravel, "Optical coatings for high power lasers," in Optical Interference Coating 2004.
2. A. Gatto, N. Kaiser, S. Günster, D. Ristan, M. Trovo and M. Danailov, "Toward resistant VUV coatings for free electron laser down to 150 nm," (submitted to Appl. Opt.).
3. H. Bercegol, P. Bouchut, L. Lamaignère, B. Le Garrec, and G. Razé, "The impact of laser damage on the lifetime of optical components in fusion lasers," in Laser-Induced Damage in Optical Materials: 2003, G. J. Exarhos, A. H. Guenther, N. Kaiser, K. L. Lewis, M. J. Soileau, and C. J. Stolz, eds., Proc. SPIE **5273,** 312–324 (2004).
4. N. Kaiser and H. Pulker, *Optical Interference Coatings* (Springer, 2003).
5. E. Welsh and D. Ristau, "Photothermal measurements on optical thin films," Appl. Opt. **34,** 7339–7253 (1995).
6. Z. Wu, M. Thomsen, P. Kuo, Y. Lu, C. Stolz, and M. Koslowski, "Photothermal characterization of optical thin film coatings," Opt. Eng. **36,** 251–262 (1997).
7. S. G. Demos and M. Staggs, "Application of fluorescence microscopy for noninvasive detection of surface contamination and precursors to laser damage," Appl. Opt. **41,** 1444–1450 (2002).
8. A. During, M. Commandré, C. Fossati, B. Bertussi, J. Y. Natoli, J. L. Rullier, H. Bercegol, and P. Bouchut, "Integrated photothermal microscope and laser damage test facility for *in-situ* investigation of nanodefect induced damage," Opt. Express **11,** 2497–2501 (2003).
9. M. Commandré and P. Roche, "Characterization of optical coatings by photothermal deflection," Appl. Opt. **35,** pp. 5021–5034 (1996).
10. V. Loriette and C. Boccara, "Absorption of low-loss optical materials measured at 1064 nm by a position-modulated collinear photothermal detection technique," Appl. Opt. **42,** 649–656 (2003).
11. A. During, C. Fossati, and M. Commandré, "Photothermal deflection microscopy for imaging submicronic defects in optical materials," Opt. Commun. **230,** 279–286 (2004).
12. C. Amra, "Light scattering from multilayer optics. II. Application to experiment," J. Opt. Soc. Am. A **11,** pp. 211–226 (1994).
13. S. Maure, G. Albrand, and C. Amra, "Low-level scattering and localized defects," Appl. Opt. **35,** 5573–5582 (1996).
14. A. Gatto and M. Commandré, "Multiscale mapping technique for the simultaneous estimation of absorption and partial scattering in optical coatings," Appl. Opt. **41,** 225–234 (2002)
15. A. During, C. Fossati, and M. Commandré, "Multiwavelength imaging of defects in ultraviolet optical materials," Appl. Opt. **41,** 3118–3126 (2002).
16. S. Demos, M. Staggs, M. Yan, H. Radousky, and J. De Yoreo, "Microscopic fluorescence imaging of bulk defect clusters in KH_2PO_4 crystals," Opt. Lett. **24,** 268–270 (1999).
17. Ch. Mühlig, W. Triebel, S. Bark-Zollmann, and D. Grebner, "*In situ* diagnostics of pulse laser-induced defects in DUV transparent fused silica glasses," Nucl. Instr. and Meth. Phys. Res. B **168,** 698–703 (2000).
18. A. C. Boccara, D. Fournier, W. Jackson, and N. M. Amer, "Sensitive photothermal deflection technique for measuring absorption in optically thin media," Opt. Lett. **5,** 377–379 (1980).
19. M. Commandré and E. Pelletier, "Measurement of absorption losses in TiO_2 films by a collinear photothermal deflection technique," Appl. Opt. **29,** 4276–4283 (1990).
20. S. Tisserand, F. Flory, A. Gatto, L. Roux, M. Adamik, and I. Kovacs, "Titanium implantation in bulk and thin film amorphous silica," J. Appl. Phys. **83,** 5150–5153 (1998).
21. W. B. Jackson, N. M. Amer, A. C. Boccara, and D. Fournier, "Photothermal deflection spectroscopy and detection," Appl. Opt. **20,** 1333–1344 (1981).
22. M. A. Olmstead, N. M. Amer, S. Kohn, D. Fournier, and A. C. Boccara, "Photothermal displacement spectroscopy: an optical probe for solid and surfaces," Appl. Phys. **32,** 141–154 (1983).
23. H. A. Macleod, *Thin-film Optical Filters* (Adam Hilger, Bristol, UK, 1986).
24. D. Ristau and J. Ebert, "Development of a thermographic laser calorimeter," Appl. Opt. **25,** 4571–4578 (1986).
25. J. Lambropoulos, M. Jolly, S. Amsden, S. Gilman, M. Sinicropi, D. Diakomihalis, and S. Jacobs, "Thermal conductivity of dielectric thin films," J. Appl. Phys. **66,** 4230–4242 (1989).
26. Z. Wu, M. Reichling, X. Hu, K. Balasubramanian, and K. Guenther, "Absorption and thermal conductivity of oxide thin films measured by photothermal displacement and reflectance methods," Appl. Opt. **32,** 5660–5665 (1993).

27. H. Machlab, W. McGahan, J. Woollam, and K. Cole, "Thermal characterization of thin films by photothermally induced laser beam deflection," Thin Solid Films **224,** 22–27 (1993).
28. M. Rohde, "Photoacoustic characterization of thermal transport properties in thin films and microsctructures," Thin Solid Films **238,** 199–206 (1994).
29. S. Lee, D. Cahill, and T. Allen, "Thermal conductivity of sputtered oxide films," Phys. Rev. B **52,** 253–257 (1995).
30. E. Drouard, P. Huguet-Chantôme, L. Escoubas, and F. Flory, "$\partial n/\partial T$ measurements performed with guided waves and their application to the temperature sensitivity of wavelength-division multiplexing filters," Appl. Opt. **41,** 3192–3136 (2002).
31. L. Gallais and M. Commandré, "Photothermal deflection in multilayer coatings: modeling and experiment," Applied Optics (to be published).
32. "Test methods for radiation scattered by optical components," Norm ISO 13696:2002 (International Organization for Standardization, 2002).
33. L. Gallais, P. Voarino, and C. Amra, "Optical measurement of size and complex index of laser damage precursors: the inverse problem," J. Opt. Soc. Am. B **21,** 1073–1080 (2003).
34. P. Torchio, A. Gatto, M. Alvisi, G. Albrand, N. Kaiser, and C. Amra, "High-reflectivity HfO_2/SiO_2 ultraviolet mirrors," Appl. Opt. **41,** 3156–3261 (2002).
35. N. Leclerc, C. Pfeiderer, J. Wolfrum, K. Greulich, W. P. Leung, M. Kulkarni, and A. C. Tam, "Transient absorption and fluorescence spectroscopy in fused silica induced by pulsed KrF excimer laser irradiation," Appl. Phys. Lett. **59,** 3369–3371 (1991).
36. N. Kuzuu and M. Murahara, "Excimer-induced emissions bands in fused quartz," Phys. Rev. B **47,** 3083–3088 (1993).
37. M. Watanabe, S. Juodkasis, H. B. Sun, S. Matsuo, and H. Misawa, "Luminescence and defect formation by visible and near-infrared irradiation of vitreous silica," Phys. Rev. B **60,** 9959–9964 (1999).